POLITECNICO DI MILANO

School of Industrial and Information Engineering

Master of Science in Mechanical Engineering

POLITECNICO
MILANO 1863

ANALYTICAL MODEL FOR WHEEL PROFILE WEAR

Supervisor : Prof. Stefano Bruni

: Dr. Egidio Di Gialleonardo

Author:

Rama Primadi Putera, 894136, 10592327

Academic year 2020/2021

Acknowledgements

I would like to express my sincere gratitude to Prof. Stefano Bruni who has guided me during my thesis work. His guidance and supportive feedbacks helped me in all the time of research and writing of this thesis. I would also like to thank Dr. Egidio Di Gialleonardo, for his time and his supportive help through this work. I can hardly describe how his invaluable advice and encouragement have been most helpful and beneficial so that I am able to finish this thesis.

Additionally, I would also like to extend my thanks to all my professors, tutor, and colleagues during my master's study for sharing their expertise and knowledge, I hope I could become a better person in the future.

My gratitude also goes to my parents and family who always support me in every way they could. This accomplishment would not have been possible without them. Thank you.

Milano, December 2021

Rama Primadi Putera

"The best of people are those that bring most benefit to the rest of mankind."

Muhammad pubh as narrated by Ahmad, tabarani, and Daruqutni

Abstract

This thesis has the aim to check the effect of gauge widening on wheel wear and on RCF damage. The purpose is to provide technical information about RCF damage on the wheel using two different methods, the first proposed by Ekberg based on Shakedown Diagram and the second by Burstow. The analysis will be performed considering two different trains, one for passenger service and the second for freight transportation. The effect of gauge widening will be analyzed also considering two different loading conditions of the freight wagon, empty and fully loaded.

Keywords: Rail-wheel contact, RCF, Ekberg, Shakedown Diagram, Burstow, RCF Damage Index, Contact Stress, Tγ, Rail Profile, R260, R350 HT, Derailment, Y/Q

Estratto in lingua italiana

Questa tesi ha lo scopo di verificare l'effetto dell'allargamento del calibro sull'usura delle ruote e sui danni RCF. Lo scopo è fornire informazioni tecniche sui danni RCF sulla ruota utilizzando due diversi metodi, il primo proposto da Ekberg basato sul diagramma Shakedown e il secondo da Burstow. L'analisi verrà effettuata considerando due diversi treni, uno per il servizio passeggeri e il secondo per il trasporto merci. L'effetto dell'allargamento della sagoma sarà analizzato anche considerando due diverse condizioni di carico del carro merci, vuoto ea pieno carico.

Keywords: Contatto rotaia-ruota, RCF, Ekberg, diagramma Shakedown, Burstow, indice di danno RCF, sollecitazione da contatto, Tγ, profilo rotaia, R260, R350 HT, deragliamento, Y/Q

Table of Contents

List of Figures

List of Tables

List of Symbols

Tγ	= Wear Index
C_{ij}	= Kalker creep coefficient (from tabulated data)
F_x	= Longitudinal creep force
F_y	= Lateral creep force
F_{spin}	= Spin creep force
G	= Shear modulus
c	= size of contact ellipse
γ_x	= Longitudinal creepage
γ_y	= Lateral creepage
φ	= Spin creepage
p_o	= Contact pressure
k	= Shear yield stress
F_T	= Tangential resultant creep force
F_z	= Vertical force
μ	= Utilized friction coefficient
v	= Normalized vertical force
FI_{surf}	= Fatigue index by shakedown diagram
α	= Geometrical dimension for Prud'homme
Q_o	= Static vertical wheel-rail contact

CHAPTER 1 INTRODUCTION

Technology develops exponentially in recent years, especially in railway vehicle. In commercial operation, the high-speed train currently can run with more than 400 $\frac{km}{h}$. Those high-speed train can exceeds because using maglev (magnetic levitation) set of train and rail. However, with the specific condition where each station is every four kilometer like mobility inner city, electrical-powered train with metal rail are still fit in terms of cost. Even diesel-powered train still around with best usage of freight transportation in long haul.

Nowadays, the recent forward-thinking researchers have been focusing to improved safety, comfort, performances, and cost not only for railway vehicle, but also for railway infrastructure. Wheelset derailment due to flange climb is one of the most dangerous occurrences affecting the ride safety of railway vehicles and needs to be prevented by a combination of good design criteria and appropriate vehicle operation practice. During vehicle service, safety against derailment must be ensured by setting appropriate maintenance standards for the rolling stock (control of wheel profile wear). Also, mainly poor quality of track geometry and track irregularities will cause derailment if specific condition (for example velocity of train or tight curving radius) are met.

Wheel and rail profiles are designed to support the desired performance of the wheel-rail system. The performance criteria include vehicle behavior on the track, for instance derailment safety, running stability, and ride comfort. The contact of wheel and rail (contact stress) is very intriguing idea, because with the small area (consider area of circle with diameter 14 milimeter for example) will generate high stresses on the rail thus during operation the wheels and rail will deteriorate over time. This deterioration phenomena may alter the shape of the profiles and endanger adequate performance. The ability to predict this process by numerical simulation would thus be of assistance in the optimum design of the wheel-rail interface.

Two main causes of the damage of wheel and rail, which is wear and Rolling Contact Fatigue (RCF), both determine the lifetime of railway wheel and rail. Wear index (Tγ) can be used as an indicator for wear, but it can be also used for quantifying RCF damage, in fact at high wear index, RCF does not have the opportunity to develop further, cracks can initiate but will be worn off due to the high wear index rate and will not be able to propagate beneath the surface. Take into consideration, when optimizing to reduce the wear index, RCF can become the dominant problem. RCF has emerged as a governing reason for rail replacement and maintenance and for rail failure and safety concerns.

A review of the types of RCF defects on wheels and rails, causal mechanisms, and monitoring and maintenance practices has been undertaken for the purpose of identifying gaps and the most pressing areas for research and development. Prominent models used in rolling

contacts for understanding crack initiation are the Shakedown Limit by Ekberg et al. [1,2]. Their implementation is relatively straightforward, but opportunities exist for better characterizing the material properties upon which they depend. On the other hand, RCF Damage Index by Burstow [3] can predict RCF model for rails. Hence, two existing RCF prediction models (Ekberg and Burstow), have been analyzed.

The aim of this thesis is to analyze the effect of gauge widening on wear and both RCF prediction. The structure of this thesis is briefly listed below.

- In second chapter, the state of art regarding definition of the models for wear and RCF are illustrated
- In third chapter, listed simulation models, input data as well as parameter to analyze
- In fourth chapter, the results of the simulation are presented, with different curve radius and rail material
- Conclusive remarks are provided in fifth chapter.

CHAPTER 2 STATE OF THE ART

Damage of wheels and rails has been of concern in the railway business for several decades [4]. With current trends towards increased axle loads and higher speeds, the phenomenon becomes even more accentuated despite significant achievements in material development and vehicle design. The focus on infrastructure maintenance and rolling stock life cycle costs also draws attention to the possibilities of wear control. In general, the course of events usually called wear is a complicated process involving several modes of material deterioration and contact surface alteration. Thus, material removal or relocation, plastic flow, and phase transformation may take place at, just below, or in-between the contacting surfaces. The railway operation imposes cyclic loading on the wheel and rail. Depending on the wheel load, contact stress distribution, and subsurface stress, plastic deformation, and shakedown as well as RCF may occur. The initiation of fatigue cracks in steel is again a threshold phenomenon.

On second chapter, starting with discussion to understand the actual force on the wheel-rail interface, then to check the criteria about safety in derailment and running in curves. After that, with the cyclic loading to operate (below yield of material), it will generate wear index ($T\gamma$). Last, to see the effect of force on the wheel-rail interface, RCF method both with Burstow [3,5] and Ekberg [1,2] models will be presented.

2.1 WHEEL-RAIL INTERFACE

The contact conditions experienced during the wheel-rail interaction show considerable variations owning to vehicle and operation status, track properties, and external influences. The friction conditions may vary from adequate adhesion with dry and clean steel-on-steel surfaces to low adhesion due to contamination, humidity, and applied friction modifiers. In general terms, wheel-rail contact mechanics is a vast area ranging from overall vehicle dynamics and assessment of global contact forces to micromechanics of the surface materials in contact. The first part addresses the contact stress and corresponding stress distributions, whereas the second deals with the relationship between creep and creep forces.

2.1.1. Contact Stress

In railway applications, the contact stress problem involves both normal and tangential loads. In the general case the corresponding normal and shear stress distributions are not independent. Traditionally, Hertz's theory of elliptic contact [6] has been applied to the normal problem, however, some of the underlying assumptions may be violated in wheel-rail application: (i) locally the material may experience plasticity, and (ii) the extension of the contact area may not be small in comparison with body radii close to the gauge corner. Carter [7] described a simple 2D contact surface, but he was the first to give a rather adequate expression of the force relative to the creepage in the longitudinal direction. His method of

describing the stresses in the adhesive zone was used until 1960s. For tangential loads, Kalker [8] and Johnson [9] can give an expression of the creepage stiffness introducing variable coefficients depending on the b/a ratio of the contact ellipse. The wheel-rail contact is a rolling friction contact, with an area of adhesion and an area of slip which appears progressively as the slip speed increases. Comparison of Carter and Kalker can be seen in Figure 1, with x-axis for longitudinal creepage and y-axis is for ratio of creep force and normal force (traction).

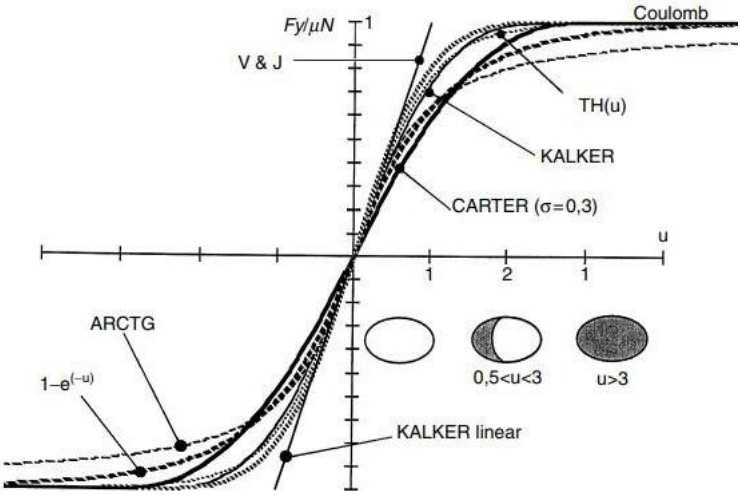

Figure 1 "Heuristic" expressions used for the saturation and physical meaning of the different parts [10]

2.1.2. Creep Force and Creepage

In the case of a Hertzian contact, the creep forces are a function of the relative speeds between rigid bodies near the contact point, the creepages. In the 1960s, Kalker developed a linear theory, with the general expression of the creep forces takes into account stiffness coefficients C_{ij} expressed in the linear theory of Kalker [7] by:

$$\begin{Bmatrix} F_x \\ F_y \\ F_{spin} \end{Bmatrix} = Gc^2 \begin{bmatrix} C_{11} & 0 & 0 \\ 0 & C_{22} & cC_{23} \\ 0 & -cC_{11} & cC_{33} \end{bmatrix} \begin{Bmatrix} \gamma_x \\ \gamma_y \\ \varphi \end{Bmatrix} \tag{2.1}$$

$$c = \sqrt{ab}$$

Where a, b are the semi-axes of the contact ellipse, F is a creep force, G is a material shear modulus, and γ is a creepage or creep ratio. Kalker tabulated the creep coefficients C_{ij} being functions of Poisson's ratio and the ratio a/b of the contact ellipse semi-axes. Kalker's linear theory is extensively used in practice in rail vehicle dynamics applications, both directly in linear simulations, where the creep is sufficiently small, and as basis for nonlinear extensions. Further developments resulted in a generalized theory for two arbitrary bodies in contact. The bodies were still described as elastic half-spaces, but the contact geometry was not

restricted to the elliptic case. Kalker also provided a numerical implementation using boundary element discretization [11], This code, CONTACT, is often used as reference but requires too much computer time for on-line use in vehicle dynamics simulation. Kalker's numerical implementation CONTACT [11] may be viewed as the exact solution, still relying on the half-space assumption but not restricted to quasi identical bodies and elliptic contact.

2.2 RUNNING SAFETY OF RAILWAY VEHICLE

Railway derailments due to loss of the lateral guidance at the wheel and rail interface may be classified into three major causes: wheel flange climb, rail rollover, and track panel shift [10]. In the following the derailment criteria and track-shift force criteria will be briefly discussed.

2.2.1. Wheel Flange Climb

Wheel flange climb derailments are caused by wheels climbing onto the top of the railhead then further running over the rail, as shown on Figure 2. Wheel climb derailments generally occur in situations where the wheel experiences a high lateral force combined with circumstances where the vertical force is reduced on the flanging wheel which is in curves. The wheels on the outer rail usually experience a base level of lateral force to vertical force ratio (L/V or Y/Q) that is mainly related to: curve radius, wheel-rail profiles, bogie suspension characteristics, and vehicle speed. Nonetheless, wheel flange climb can also occur on tangent track (straight track) when track irregularities and vehicle lateral dynamic motion are severe, such as during vehicle hunting and aggressive braking.

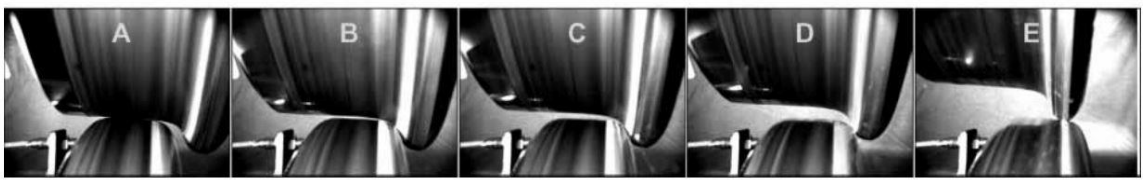

Figure 2 Evolution of Wheel Derailment [12]

Several flanges climb safety criteria have been proposed. These criteria are related to either L/V ratio limits or time/distance limits (applied to limit the exceeding duration of the L/V ratio limit, in time/distance scale). The wheel climb would be very likely to occur as both the L/V limit and time limit are exceeded. For simplicity, Nadal single-wheel L/V limit criterion is presented here [10].

Nadal assumed that the wheel was initially in two-point contact with the flange point leading the tread point. He concluded that the wheel material at flange contact point was moving downwards relative to the rail material, due to the wheel rolling about the tread contact, as illustrated in Figure 3. Based on that, equation 2.2 and 2.3 can be derived. Figure 4 display an example of a single-axle wheel climbing. These are the results from simulations using NUCARS™ and flange climb tests conducted using the Association of American Railroads Track-Loading Vehicle [13]. Figure 4 also indicates that for large wheelset angles of attack (about 10 mrad) derailments occurred at Nadal's value (more or less value of 1.2), in which this limit is being used for the calculation in chapter four. On the other hand, considering small angles of attack, Nadal criterion is found to be conservative.

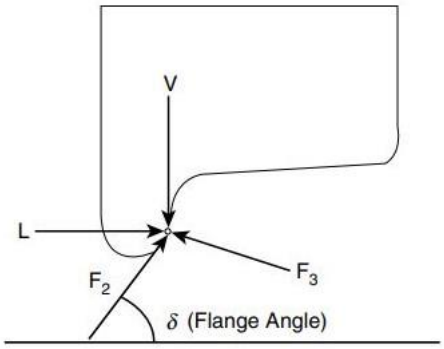

Figure 3 Force at Flange Contact Location [10]

$$\frac{L}{V} = \frac{\tan\delta - \frac{F_2}{F_3}}{1 + \frac{F_2}{F_3}\tan\delta} \tag{2.2}$$

$$\frac{L}{V} = \frac{\tan\delta - \mu}{1 + \mu\tan\delta} \tag{2.3}$$

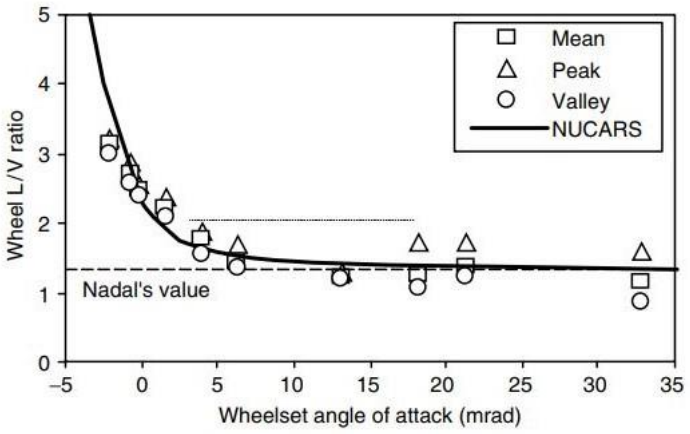

Figure 4 Effect of Wheelset angle of attack on Wheel L/V ratio limit [10]

2.2.2. Running Safety in Curves

The sum of guiding forces is relevant to assess the running safety of the vehicle because they can determine track-shift. For the sum of guiding forces, the limit used for an average value over 2 m distance is according to UIC 518 [14] and EN 14363 [15] the value according to Prud'homme [10]:

$$\sum Y_{2m} = \alpha \left(10 + \frac{2Q_o}{3}\right)[kN] \tag{2.4}$$

With α taking into account of greater variations in geometrical dimensions and the state of vehicle maintenance (α = 0.85 for freight wagons, α = 1.0 for other vehicles), and Q_o static vertical wheel-rail contact force. The criterion is valid on straight track as well as in curves. However, in curves the dynamic value excited by irregularities is superimposed by the steady-state value, which makes this limit more critical, mainly when running at high speed through curves with a tight radius. To reduce the sum of guiding forces, both steady state as well as the dynamic value of the track shifting force must be as low as possible. The sum of all steady-state track shifting forces acing on the vehicle is defined by the product of vehicle mass and lateral acceleration, which is a function of curve radius and cant deficiency. An optimization is limited to an equal distribution of the forces on wheelsets.

2.3 WEAR INDEX AND RCF DAMAGE INDEX

RCF predictor by Burstow is based on the energy dissipation in the wheel–rail contact [3,5]. This model has been mainly developed to predict RCF on rails. The model combines the longitudinal and lateral creep forces (F_x *and* F_y $[N]$) with the corresponding creep (γ_x *and* γ_y) to calculate the wear number (Tγ):

$$T_\gamma = F_x\gamma_x + F_y\gamma_y \tag{2.5}$$

The fatigue damage depends on the value of the wear number, Tγ [N], according to the damage function in Figure 5. The RCF Damage Index, which is defined here as the proportion of the fatigue life of the material for that specific contact condition. For each contact position, the damage index can be summed, and fatigue will occur when unity is reached for the total DI. The model also considers the influence of wear (negative slope in Figure 5). For high Tγ ($T_\gamma > 65\ N$), wear starts to dominate and for $T_\gamma > 175\ N$, the wear rate is even higher than the crack growth, resulting in no RCF damage at all. The main disadvantage of this RCF prediction model is its empirical nature and need for recalibration for new applications. In

addition, the contact pressure is not explicitly considered, which may influence the formation of RCF cracks [5]. Another disadvantage is that spin creepage is not explicitly included in the wear number, Tγ. Especially for contact positions on the gauge corner of the rail, where spin creepage can be high and cracks often occur, it can make a difference. Curve in Figure 5 may be adjusted considering different wheel and rail steel grades.

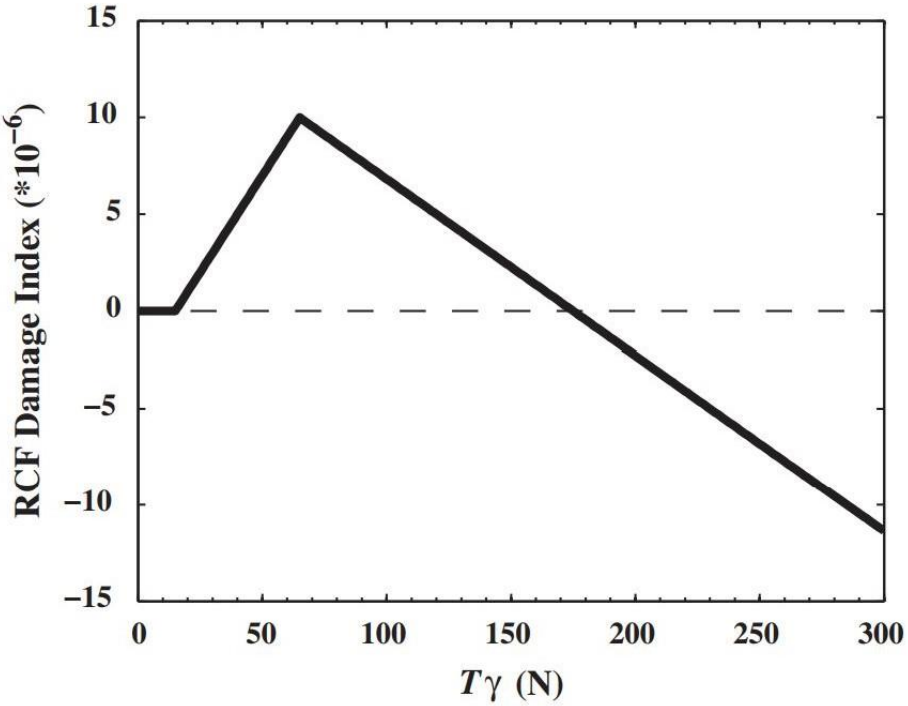

Figure 5 RCF Rail Damage Index [3]

2.4 EKBERG MODEL FOR RCF

Ekberg et al. [1,2] developed a prediction model for surface initiated RCF on railway wheels, which is based on shakedown theory [16,17]. The occurrence of RCF depends upon the pressure and the creep forces in the contact patch. If the stresses exceed the so-called 'shakedown limit', surface cracking will occur due to accumulated plastic strain. The shakedown diagram is often used to compare the contact conditions with the shakedown limit (Figure 6). The location of the limit in the shakedown diagram is a function of the maximum contact pressure ($p_o \; in \; [\frac{N}{m^2}]$) divided by the material yield stress in shear ($k \; in \; [\frac{N}{m^2}]$), and the utilized friction coefficient was defined as the quotient between the tangential resultant creep force ($F_T \; [N]$) and the vertical force ($F_z \; [N]$):

$$\mu = \frac{F_T}{F_z} = \frac{\sqrt{F_x^2 + F_y^2}}{F_z} \tag{2.6}$$

Where $F_x and\ F_y$ are respectively the longitudinal and lateral creep force in [N] The equation for the boundary curve (BC in Figure 6) is defined as:

$$v = \frac{1}{\mu} \tag{2.7}$$

A surface fatigue index (FI_{surf}) was defined, which can be seen as a measure for the probability of RCF initiation:

$$FI_{surf} = \mu - \frac{1}{v} = \mu - \frac{k}{p_o} \tag{2.8}$$

The fatigue index (FI) depends on to what extent the shakedown limit has been exceeded. The FI is the horizontal distance in the shakedown diagram between the working point of the contact conditions, and the shakedown limit. Damage is assumed to occur for $FI_{surf} > 0$. A disadvantage of RCF prediction model is that the applied shakedown is derived under conditions of full slip. The contact on the flange of a wheel is often in full slip; the contact on the tread, however, is often in partial slip. So, for these contact conditions, the model might be invalid. It is shown that for line contacts and for a fixed utilized friction coefficient, the shakedown limit for contacts in partial slip is lower than for contacts in full slip [16]. However, it is also mentioned that the damaging effect of partial slip in point contact is expected to be not as severe as in line contact. In this study, it is therefore assumed that the RCF model, based on shakedown diagram, can also be applied on tread contacts where partial slip is quite common. Another disadvantage of this model, which has been mentioned [3], is that the shakedown diagram does not explicitly take the creepage in the wheel-rail contact into account, though creepage can be an important variable in determining fatigue life. Besides, the model does not take the possible influence of wear into account which can also be seen as a disadvantage [18]. However, the model can be applied in combination with a separate wear model, RCF Damage Index by Burstow for example.

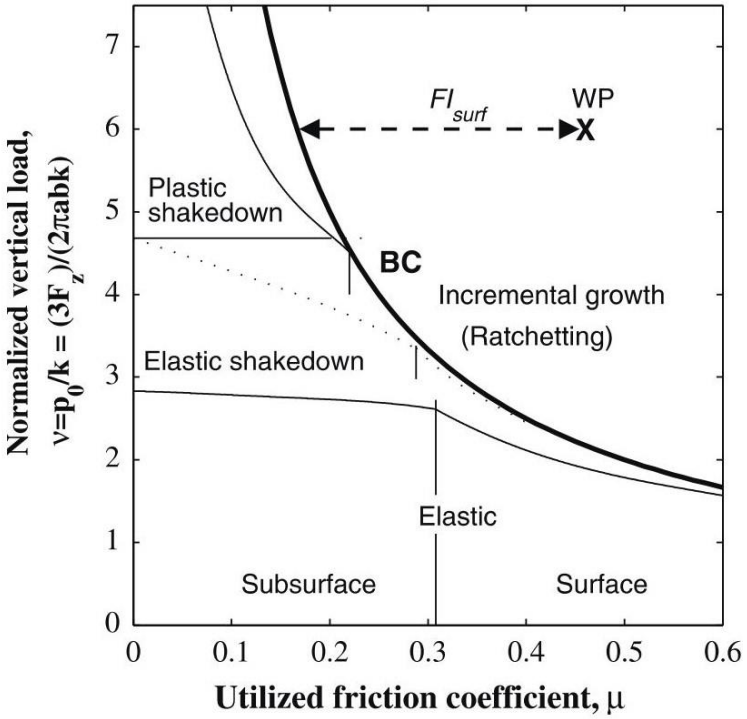

Figure 6 Shakedown Diagram with working point (WP) indicated by 'X' [2]

CHAPTER 3 TRAIN MODEL AND INPUT DATA

For studying the effect of gauge widening on wear and rolling contact fatigue (RCF) for railway wheels running on a specific line and/or for rails in a specific curve, results of three different models have been combined: a three-dimensional multi-body model for dynamic simulations, a wear model and an RCF model. The dynamics simulations of the vehicle–track interaction provided the forces which the wheel and rail profiles could experience. The output from these simulations (forces, creepages, semi-axes of the contact ellipse) were input to the wear model, which calculates the amount of wear on the wheel profiles, and input to the RCF prediction model, which calculates an index associated to the probability of crack propagation. Two different trains, passenger train (TA) and freight train (TCA) are used for studying the effect of gauge widening. Table 1 below shows the data of curve for standard gauge and parameter respectively, with two different radius (R175 and R250).

Table 1 Overview of Simulated Curve for Standard Gauge

train	length curve (m)	radius (m)	speed (km/h)
TA	300	175	68.04
	300	250	81.36
TCA	300	175	50.76
	300	250	68.04

All the simulation started with tangent track, transition track, curve track, transition track, and tangent track in the end. However, the calculation in the chapter four, are only taking value when in curve track (where the force is highest compared to tangent and transition track), with the sampling time 2ms as shown on Parameter Data Table 2 below. Gauge width for standard gauge is 1435 mm, and for gauge widening at radius 175 is 1455 mm, as for radius 250 is 1440 mm. Passenger train are simulated with eight wheelset (two train carbody), with load of 79 kN for each wheel, while freight wagon with four wheelset (one train carbody) with fully loaded (TCAL) is 117 kN ton and 33 kN ton in tare condition (TCAT) for each wheel. Rail material R260 and R350 HT are used with material strength 880 and 1175 MPa correspondingly. Coefficient of 0.33 from rail material strength are used [3], for calculation shear yield stress as an input for Burstow Damage Index, with 290 MPa for shear yield stress material R260 and 387 MPa for R350 HT.

Table 2 Parameter Data

Parameter	
Gauge width (mm)	1435 (ST), 1455 (GW for R175), 1440 (GW for R250)
Load for each wheel (kN)	79 (TA), 117 (TCAL), 33 (TCAT)
Rail material strength (MPa)	880 (R260), 1175 (R350 HT)
Rail shear yield stress (MPa)	290 (R260), 387 (R350 HT)
Sampling time (ms)	2

CHAPTER 4 SIMULATION

To understand the effect of different type of train, rail profile, rail material, and curve, several parameters are used in the simulation as shown in Table 3. Two sub-categories for Freight Train are fully loaded (PC-L) and in tare conditions (Tara-T). One category for Passenger Train (TA) and two for Freight Trains (TCA), making in total three type of trains to compare (TA, TCAL, TCAT).

Table 3 List of Parameters

Parameter	
Rail Profile	Standard (ST) and Gauge Widening (GW)
Rail Material	R260 and R350 HT
Curve (meter)	Radius 175 and Radius 250
Train	Passenger (TA) and Freight Train (TCA)
Sub Load for Freight Train	With Load-PC (L) and Without Load-Tara (T)

4.1 SAFETY PARAMETERS

Based on chapter 2.2, for train to running in comfort and able to deliver the goods or passenger into the destination safely, there are many criterions that train should fulfill while running. especially in curve where the lateral force is much higher than in tangent track, and if not assess correctly, will failed (derail). Two parameters many researchers used are Y/Q limit (using Nadal's criterion) and ∑Y (sum of lateral forces).

4.1.1. Y/Q Results

acquired from chapter 2.2.1, from Nadal's criterion we can use 1.2 as Y/Q limit. The value that shown in Table 4 below are generated in the leading axle (1st axle) and in outer wheel while curving, that is the flanging wheel, so the one experience larger Y/Q. Maximum value is 0.591 with TCAT type of train, gauge widening and radius 175, and this value is lower than 1.2 as Y/Q limit. Now all the train in the simulation are running in safety region (no derailment). In addition, all three cases of train have an angle of attack with range of -0.6 mrad to 12.6 mrad, and based on Figure 4, we can say that Nadal's criterion is even more conservative.

Table 4 Maximum ratio Y/Q Result

	TA	TCAL	TCAT
ST (R175)	0.517	0.505	0.574
GW (R175)	0.535	0.522	0.591
ST (R250)	0.453	0.398	0.527
GW (R250)	0.450	0.390	0.525

4.1.2. Sum of Lateral Force

Based on Prud'homme from Chapter 2.2.2, the limit ∑Y are calculated from static wheel force Q_o, and α equal to 0.85 for Freight Train (TCAL and TCAT) and 1 for Passenger Train (TA) as a geometrical input. Then compared the limit with highest Y on rail wheel contact, which is leading axle (1st axle), that can be seen on Table 5. Value of Y obtained from the sum of two products, lateral force of inner wheel and outer wheel while curving. All the Y are lower than the limit for all train cases, with TA on Radius 175 of Standard Gauge having closest to the limit (45.9% from the limit value).

$$\sum Y_{2m,limit} = \alpha \left(10 + \frac{2Q_o}{3}\right) (in\ kN) \qquad (4.1)$$

Table 5 Limit of ∑Y based on Prud'homme (all in kN)

	TA			TCAL			TCAT		
	Q_o	$\sum Y_{lim}$	Y	Q_o	$\sum Y_{lim}$	Y	Q_o	$\sum Y_{lim}$	Y
ST (R175)	79	62.7	28.8	117	74.8	26.3	33	27.2	8.3
GW (R175)	79	62.7	28.4	117	74.8	24.8	33	27.2	7.9
ST (R250)	79	62.7	22.4	117	74.8	17.3	33	27.2	6
GW (R250)	79	62.7	21.8	117	74.8	16.4	33	27.2	6

4.2 WEAR INDEX (Tγ)

Wear Index is obtained combining all the Tγ in case simultaneous contact points are active (i.e. on the flanging wheel). The calculation of Tγ in Chapter 4.2 is the summation of Tγ at the contact patch one, two, and three. Wear Index (Tγ) is a parameter to determine how high the force acting on the rail and wheel contact that will lead into wear RCF fatigue. Figure 7 shows Tγ result for Passenger Train. Maximum Tγ will occur on the leading axle, and outer wheel, for Standard Gauge with 615 kN at Radius 175. On the inner wheel of leading axle with 348 kN at Radius 175. On the second axle, Tγ are less than 190 kN. When the gauge is widening, Tγ are slightly went up on the leading axle for about 3.7% in outer wheel and 4.3% in inner wheel, but on the second axle Tγ are dropped for about 2.2% for outer wheel and 21.9% for inner wheel.

When the Radius are increasing into 250, all Tγ value are reduced. For Standard Gauge, on leading axle with 491 kN at outer wheel and 259 kN at inner wheel. On second axle, Tγ are 57 kN and 82 kN respectively. There is little effect of gauge widening in Radius 250, only grew 0.4% in leading axle outer wheel and 1.5% inner wheel. On second axle, fell 3.5% in outer wheel and 2.4% inner wheel.

Tγ for Freight Wagon with Load are shown in Figure 8. Like Passenger Train, maximum Tγ will occur on the leading axle and outer wheel, with Tγ 648 kN for Standard Gauge at Radius 175. On the inner wheel of leading axle with Tγ 373 kN. On the second axle, Tγ are less than

180 kN. Gauge widening has little effect on Tγ, except on the second axle outer wheel where Tγ are dropped for about 25%.

When the Radius are increasing into 250, for Standard Gauge, on leading axle with 461 kN at outer wheel and 244 kN at inner wheel. On second axle Tγ are less than 100 kN. Tγ reduce 4.8% into 439 kN on leading axle at outer wheel when the gauge widening but increasing 2% into 249 kN at inner wheel. For Second axle, Tγ rose 5.7% at outer wheel but gently decrease 3.2% at inner wheel.

Figure 9 showed maximum Tγ on 1st and 2nd axle of Freight Wagon without Load. There are significant drop of Tγ when compared to Freight Wagon with load. Mostly because of lower vertical load that applied on the wheel which also less Tγ on rail-wheel contact. Maximum Tγ will occur on the outer wheel in leading axle, with Tγ 171 kN for Standard Gauge at Radius 175. Meanwhile on the inner wheel 104 kN. On the second axle, Tγ are less than 50 kN. Gauge widening has little effect on Tγ, except on the second axle inner wheel where Tγ are reduce 11.4%.

When the Radius are increasing into 250, for Standard Gauge, on leading axle with 139 kN at outer wheel and 77 kN at inner wheel. On second axle Tγ are less than 30 kN. Tγ increase 4.3% into 145 kN on leading axle at outer wheel when the gauge widening but decreasing 1.3% into 78 kN at inner wheel. For Second axle, Tγ rose 4.3% at outer wheel but gently decrease 3.7% at inner wheel. Table 6 shown a representative Tγ from Figure below. The highest Tγ value is in TCAL for tight Radius 175 with value 648 kN for ST and 651 kN for Gauge Widening. Figure 10 showed comparison of maximum Tγ (outer wheel and leading axle) for all type of train.

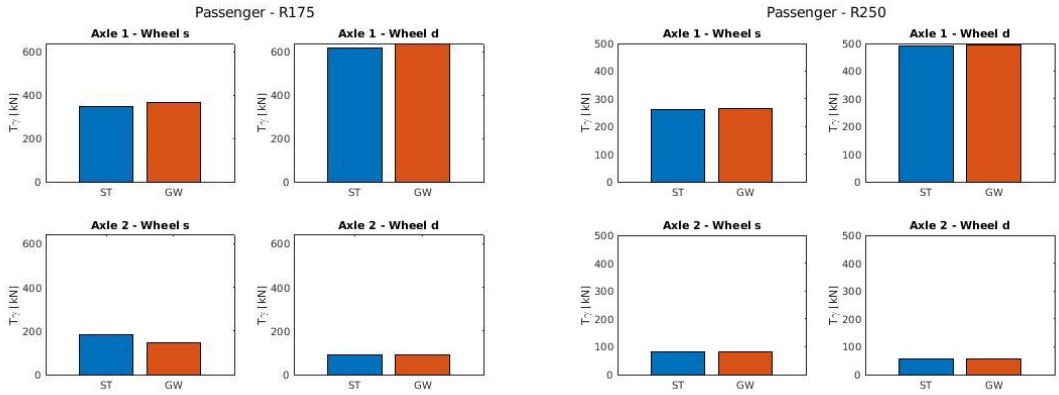

Figure 7 Tγ of TA with Axle 1 and 2 for Radius 175 (Left) and Radius 250 (Right)

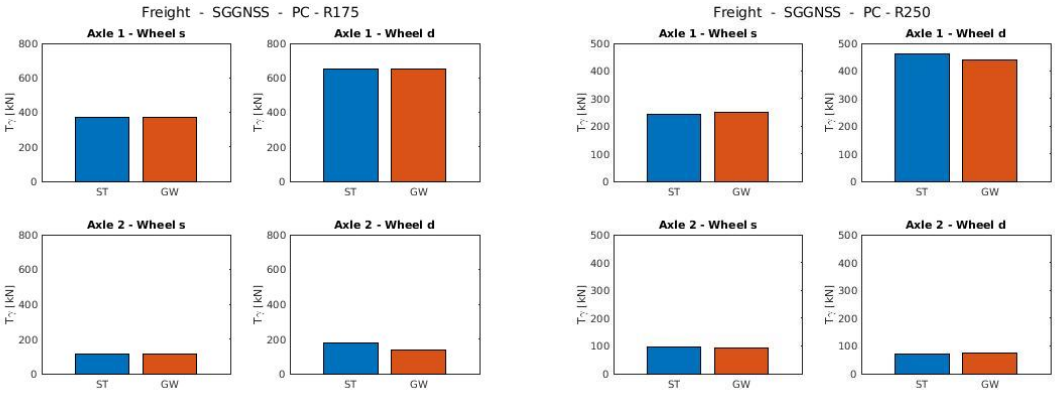

Figure 8 Tγ of TCAL with Axle 1 and 2 for Radius 175 (Left) and Radius 250 (Right)

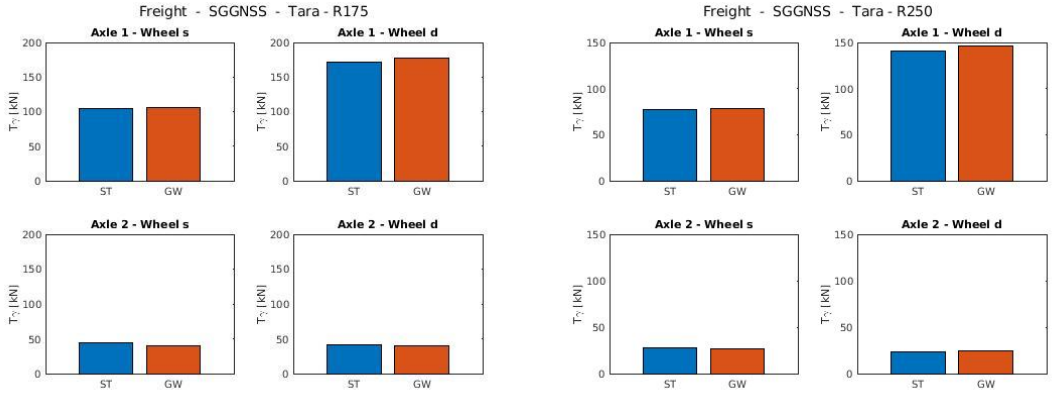

Figure 9 Tγ of TCAT with Axle 1 and 2 for Radius 175 (Left) and Radius 250 (Right)

Table 6 Maximum Tγ, ST in kN, and GW in %

	TA		TCAL		TCAT	
	(ST)	(GW)	(ST)	(GW)	(ST)	(GW)
R175 – axle 1 - left	348	4.3%	373	-1.3%	104	1%
R175 – axle 1 - right	615	3.7%	648	0.5%	171	3.5%
R175 – axle 2 -left	183	-21.9%	112	0.9%	44	-11.4%
R175 – axle 2 – right	89	-2.2%	176	-25%	41	-4.9%
R250 – axle 1 -left	259	1.5%	244	2%	77	1.3%
R250 – axle 1 – right	491	0.4%	461	-4.8%	139	4.3%
R250 – axle 2 -left	82	-2.4%	94	-3.2%	27	-3.7%
R250 – axle 2 - right	57	-3.5%	70	5.7%	23	4.3%

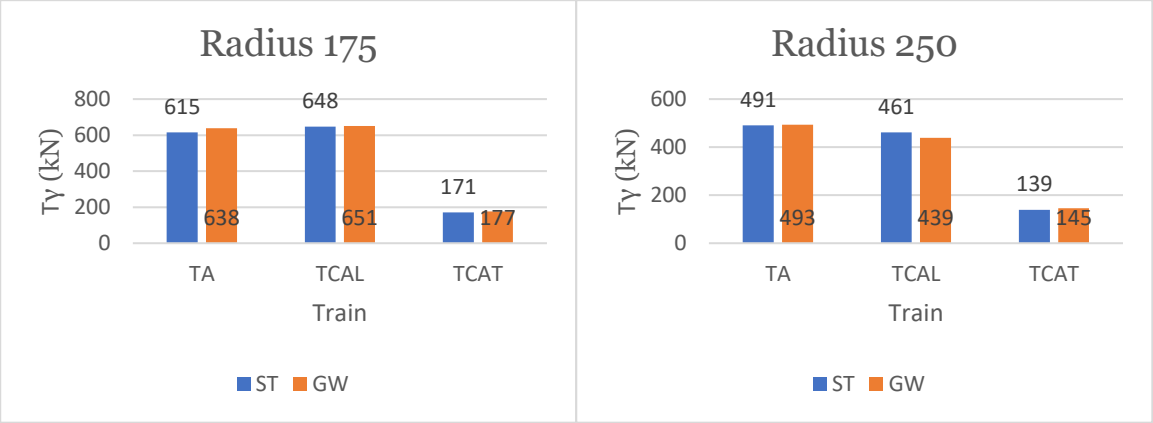

Figure 10 Tγ of Train at Outer Wheel and Leading Axle with Radius 175 (Left) and Radius 250 (Right)

4.3 RCF INDEX

There are two calculations that we can use to calculate the wear, first one is Burstow using RCF Damage Index, then Ekberg using FI_{surf} Index, both are calculated in the simulation below. Material rail strength are needed for calculation Ekberg and Burstow, with both material R260 and R350 HT data from chapter 3 are used.

4.3.1. Burstow RCF Damage Index

The Burstow Index [3,5] is computed according to chapter 2.3. It should be noted that the analysis will be performed for each possible contact point (blue line for thread, red for thread/flange, and orange for flange). The result of Burstow RCF Damage Index can be seen in Figure 11 and 12 for Passenger Train. On leading axle, there are no Burstow RCF damage index because Tγ are passing threshold for both materials. Highest Damage Index at second axle $1.08x10^{-5}$ or 55,555 cycle. If material R350 HT are used, Damage Index would reduce 75% into $0.25x10^{-5}$ or 400,000 cycle. Similar reduction also for the Freight Wagon with Load (Figure 13 and 14), where highest Damage Index at second axle $0.95x10^{-5}$ will reduce into $0.26x10^{-5}$ if material R350 HT used. Unlike Passenger Train and Freight Train with Load, Freight Train without Load (Figure 15 and 16) have a Damage Index at the leading axle. At Radius 175 outer wheel and standard gauge it produces $1.61x10^{-5}$ Damage Index, while on the second axle about one-third from leading axle, $0.58x10^{-5}$, and further reduced if material R350 HT are used, $0.46x10^{-5}$ at leading axle and no Damage Index at second axle. Table 7 and 8 shows a Damage Index comparison between two materials with specific axle, radius, and side.

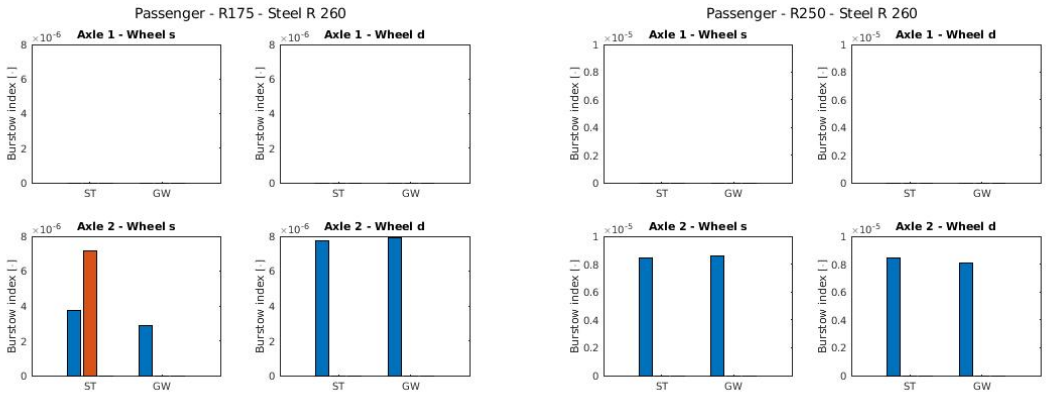

Figure 11 Burstow Index of TA with Axle 1 and 2 for Material R260, Radius 175 (Left) and Radius 250 (Right)

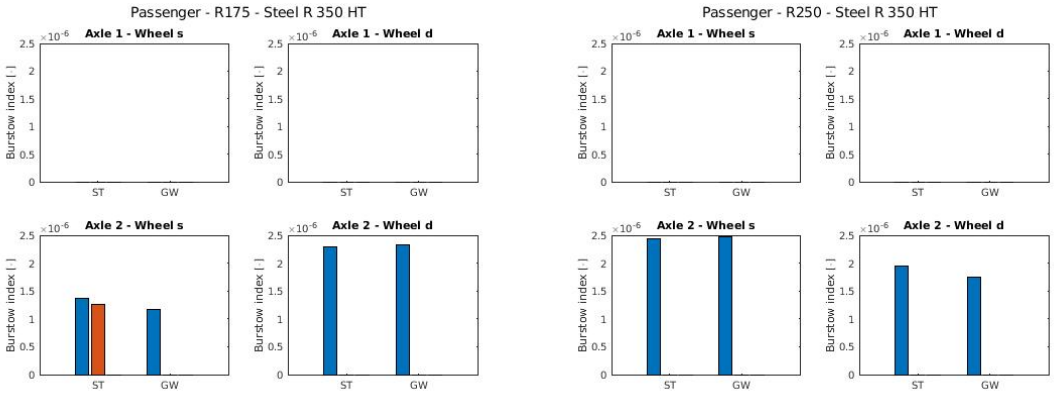

Figure 12 Burstow Index of TA with Axle 1 and 2 for Material R350 HT, Radius 175 (Left) and Radius 250 (Right)

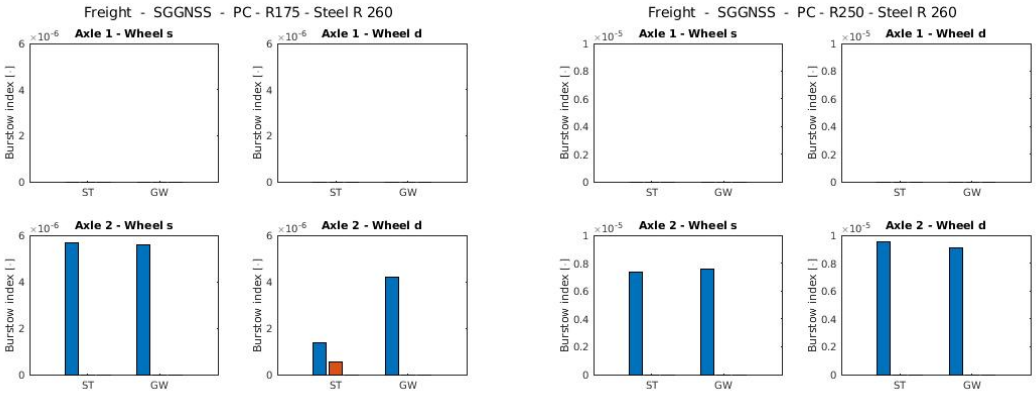

Figure 13 Burstow Index of TCAL with Axle 1 and 2 for Material R260, Radius 175 (Left) and Radius 250 (Right)

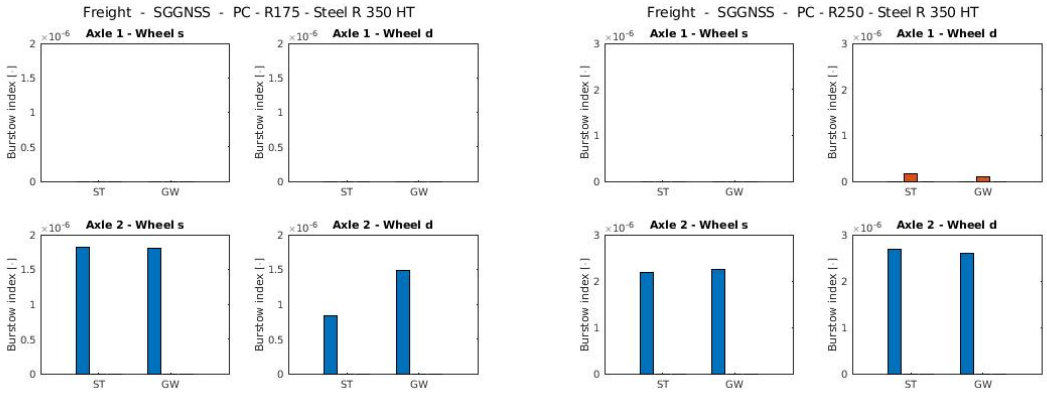

Figure 14 Burstow Index of TCAL with Axle 1 and 2 for Material R350 HT, Radius 175 (Left) and Radius 250 (Right)

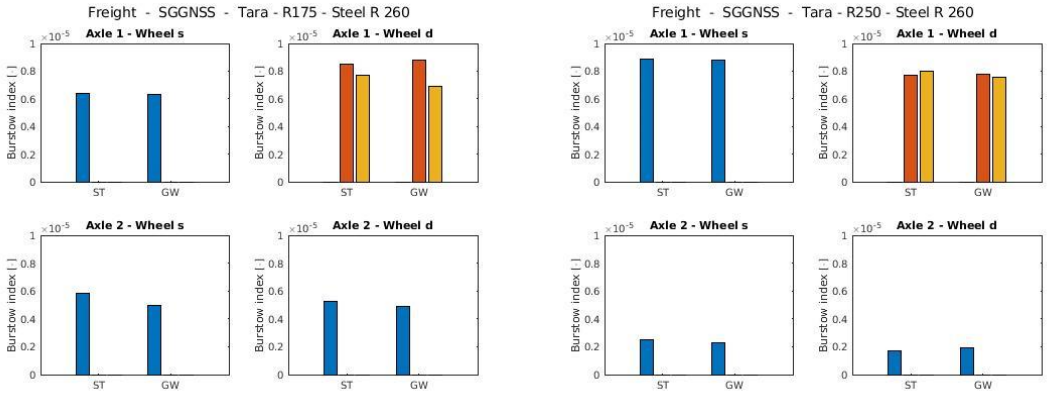

Figure 15 Burstow Index of TCAT with Axle 1 and 2 for Material R260, Radius 175 (Left) and Radius 250 (Right)

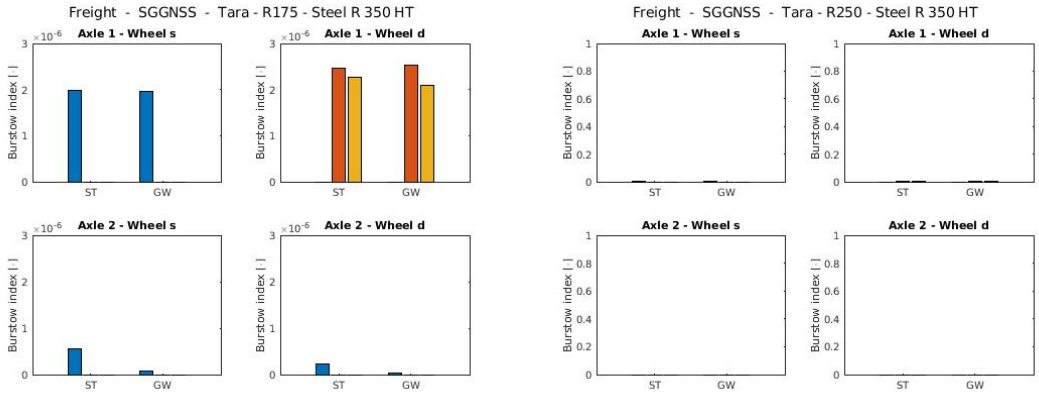

Figure 16 Burstow Index of TCAT with Axle 1 and 2 for Material R350 HT, Radius 175 (Left) and Radius 250 (Right)

Table 7 Burstow Index (in 10^{-5} Damage) for R260 Material

Axle	Radius	Side	TA		TCAL		TCAT	
			(ST)	(GW)	(ST)	(GW)	(ST)	(GW)
1	175	Left	-	-	-	-	0.64	0.63
		Right	-	-	-	-	1.61	1.55
	250	Left	-	-	-	-	0.88	0.87
		Right	-	-	-	-	1.57	1.52
2	175	Left	1.08	0.28	0.56	0.56	0.58	0.49
		Right	0.77	0.79	0.18	0.42	0.52	0.48
	250	Left	0.84	0.85	0.73	0.75	0.25	0.23
		Right	0.84	0.8	0.95	0.9	0.16	0.19

Table 8 Burstow Index (in 10^{-5} Damage) for R350 HT Material

Axle	Radius	Side	TA		TCAL		TCAT	
			(ST)	(GW)	(ST)	(GW)	(ST)	(GW)
1	175	Left	-	-	-	-	0.19	0.19
		Right	-	-	-	-	0.46	0.45
	250	Left	-	-	-	-	0.25	0.25
		Right	-	-	-	-	0.38	0.38
2	175	Left	0.25	0.11	0.18	0.17	0.05	-
		Right	0.22	0.23	0.08	0.14	0.02	-
	250	Left	0.24	0.24	0.21	0.22	-	-
		Right	0.19	0.17	0.26	0.25	-	-

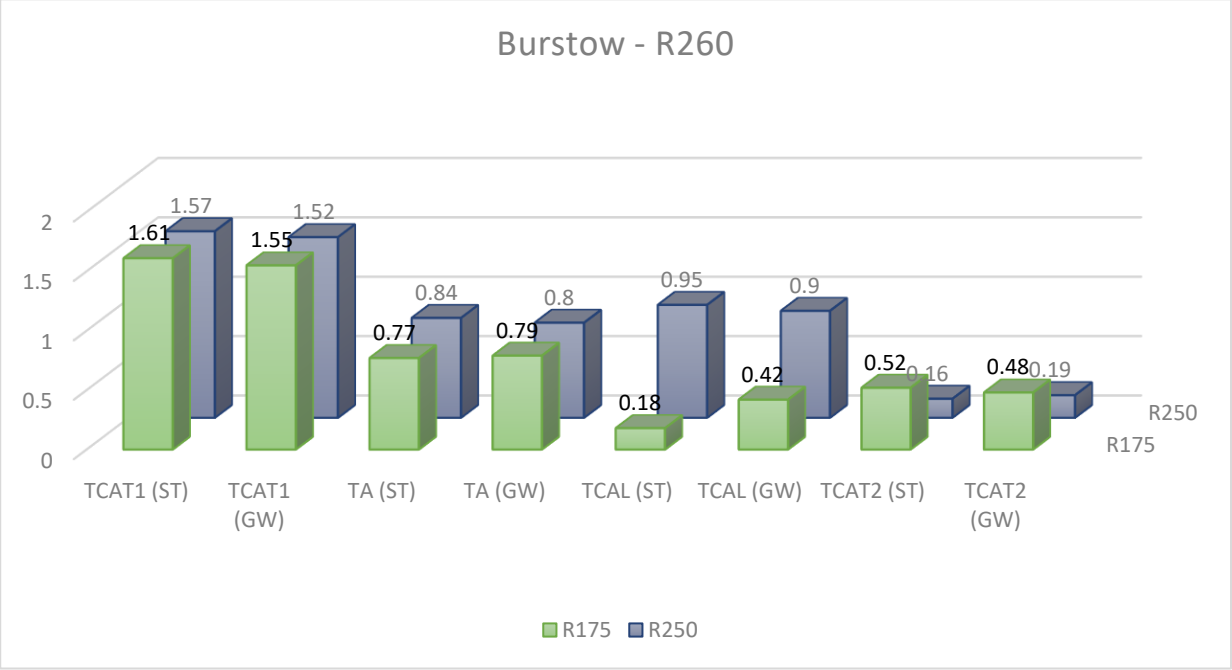

Figure 17 Ty of Train at Outer Wheel and Leading Axle with Material R260

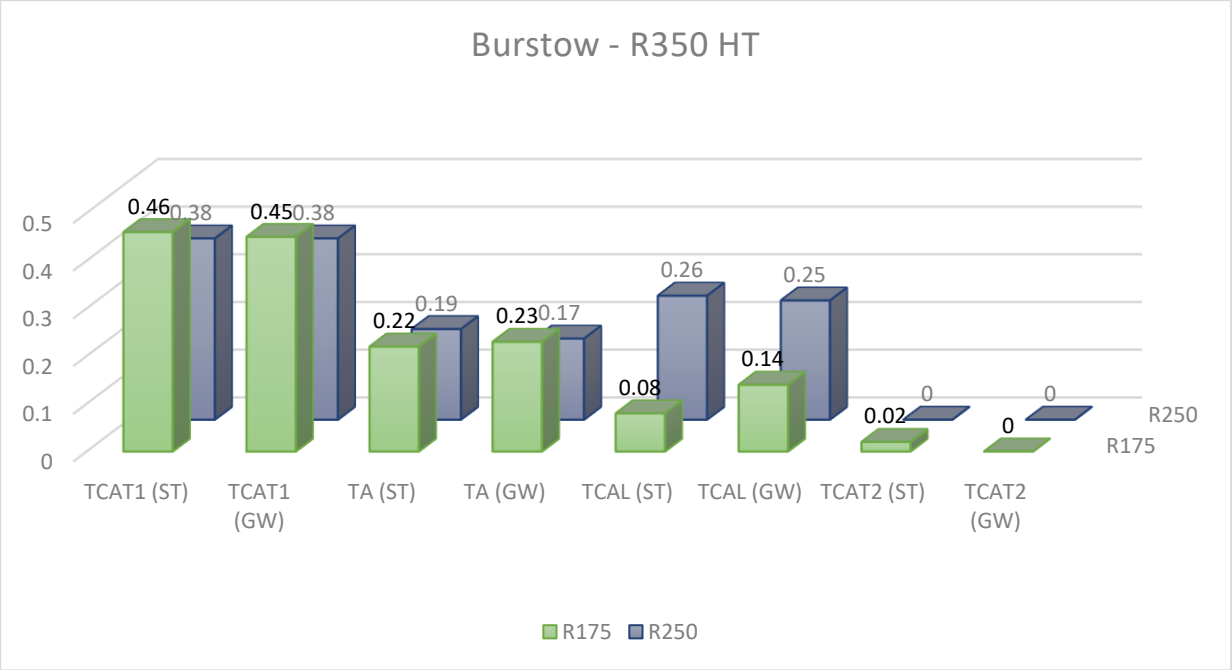

Figure 18 Tγ of Train at Outer Wheel and Leading Axle with Material R350 HT

4.3.2. Ekberg's Surface Fatigue Index

The calculation for FI_{surf} in this chapter is the summation of FI_{surf} at the contact patches one, two, and three. Figure 19 shows material R260 for FI_{surf} of Passenger Train, with maximum FI_{surf} will occur on the leading axle, and outer wheel, for Standard Gauge with FI_{surf} 0.53 at Radius 175. On the inner wheel of leading axle with 0.21 at Radius 175. On the second axle, FI_{surf} are 0.12 on the outer wheel and 0.3 on the inner wheel. When the gauge is widening, FI_{surf} are slightly went up on the leading axle for about 0.01 in outer wheel and decreasing 0.01 in inner wheel. On the second axle FI_{surf} are dropped for about 0.13 for outer wheel and 0.01 for inner wheel.

When the Radius are increasing into 250, it has little effect of FI_{surf}, except on second axle inner wheel, where there is only one contact patch compared to Radius 175 where there are two contact patches with the same value. That makes FI_{surf} reduced by 50% in Radius 250. When the gauge is widening, FI_{surf} remain same on second axle but fell on leading axle by 0.02. If R350 HT material is used it has significant effect to reduced FI_{surf} because the material can resist higher stress at contact patch. From Figure 20 it shows FI_{surf} able to reduce from 0.09 to 0.05, where for the highest FI_{surf} 0.54 will reduce to 0.45 (-16% from initial value).

Figure 21 shows FI_{surf} for TCAL of material R260. For Radius 175, highest FI_{surf} is 0.56 at outer wheel. There is small effect of reducing FI_{surf} when we increase gauge widening or increase radius, however, if we use material R350 HT (Figure 22) it will down significantly from 0.56 to 0.48 (-14% from initial value).

With reduction of load (TCAT) there are also reduction of FI_{surf} compared to TCAL. At standard gauge and radius 175, with highest FI_{surf} is 0.42 (TCAT) compared to 0.56 (TCAL), about 25% reduction from initial value (Figure 23). It will also reduce if material R350 HT are used, which decrease about 26% from 0.42 (Figure 24).

Table 9 shows FI_{surf} in the leading axle for all type of train and Figure 25 shown 3d bar diagram of maximum FI_{surf} in leading axle. From Figure 25, it has little reduction of FI_{surf} when increasing gauge or increasing radius. But if compared with Figure 26 it will reduce significantly because higher rail material strength.

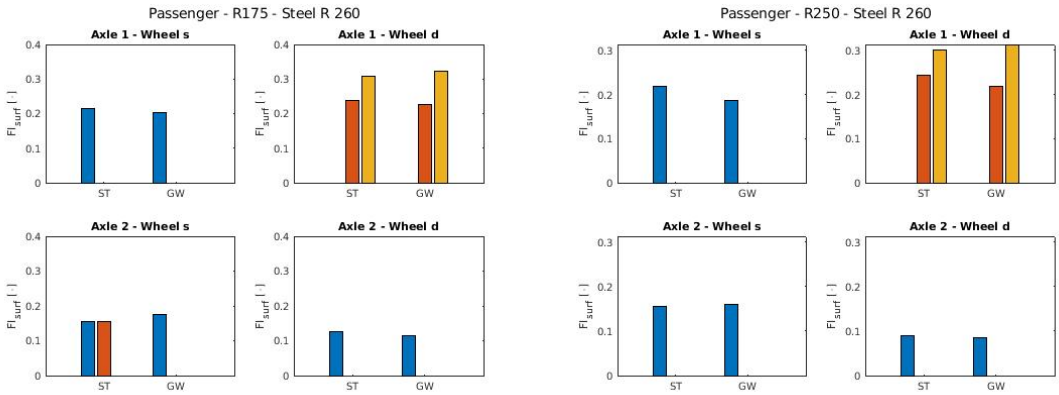

Figure 19 FIsurf of TA with Axle 1 and 2 for R260 at Radius 175 (Left) and Radius 250 (Right)

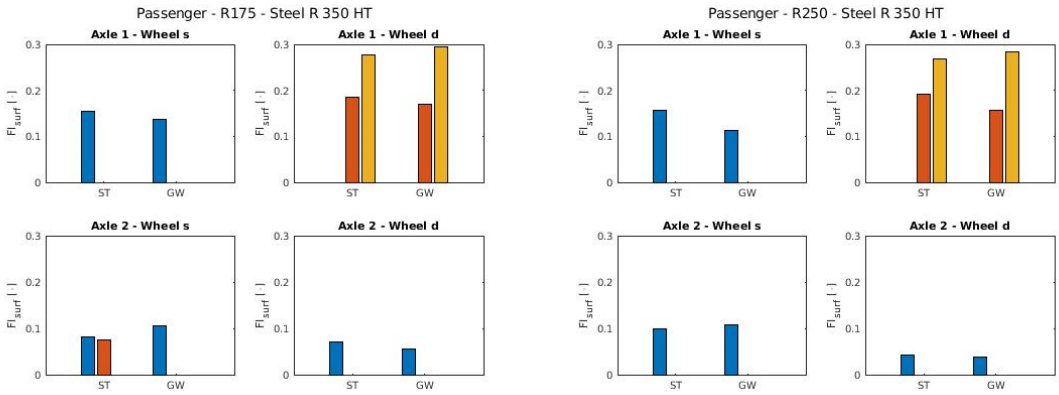

Figure 20 FIsurf of TA with Axle 1 and 2 for R350 HT at Radius 175 (Left) and Radius 250 (Right)

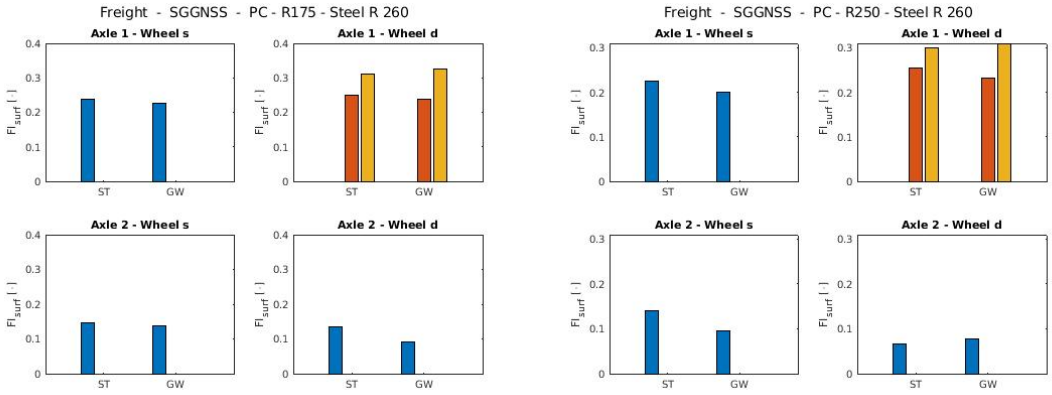

Figure 21 FIsurf of TCAL with Axle 1 and 2 for R260 at Radius 175 (Left) and Radius 250 (Right)

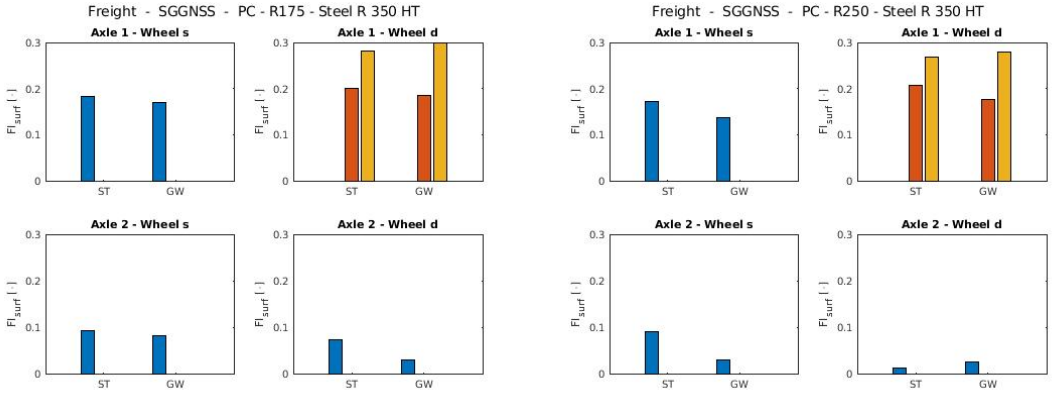

Figure 22 FIsurf of TCAL with Axle 1 and 2 for R350 HT at Radius 175 (Left) and Radius 250 (Right)

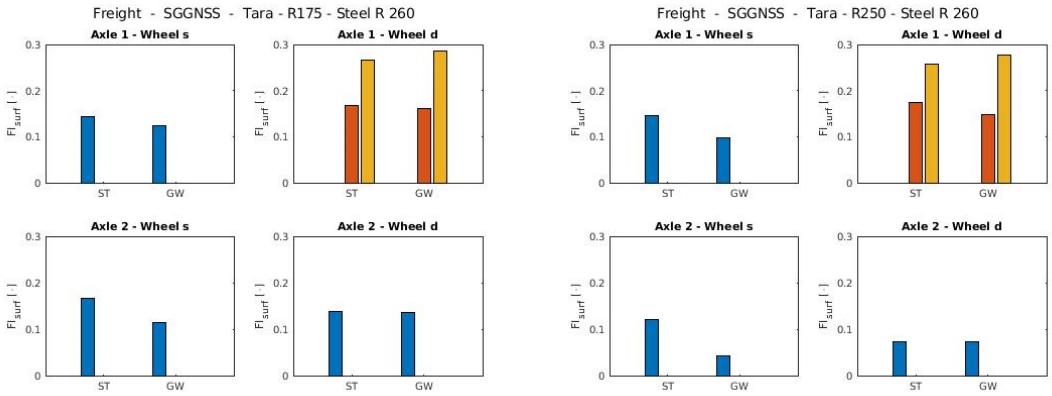

Figure 23 FIsurf of TCAT with Axle 1 and 2 for R260 at Radius 175 (Left) and Radius 250 (Right)

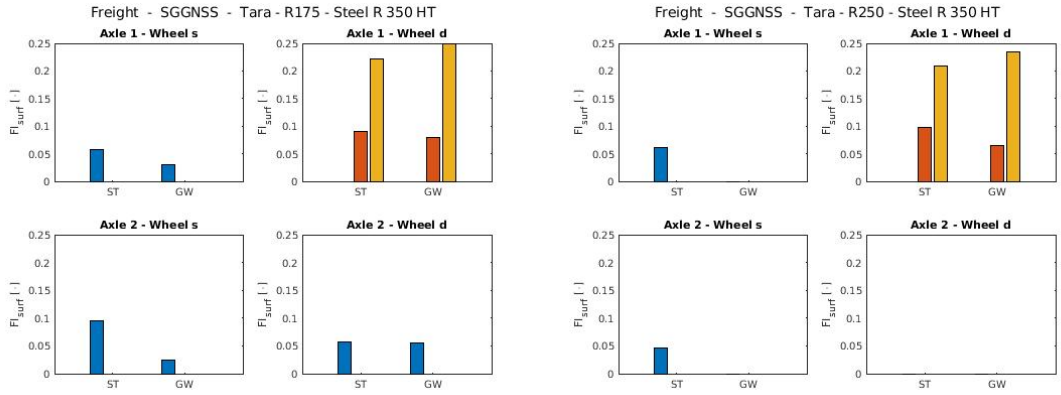

Figure 24 FIsurf of TCAT with Axle 1 and 2 for R350 HT at Radius 175 (Left) and Radius 250 (Right)

Table 9 FIsurf comparison at leading axle (no dimensional)

Material	Radius	Side	TA		TCAL		TCAT	
			(ST)	(GW)	(ST)	(GW)	(ST)	(GW)
R260	175	Left	0.21	0.2	0.23	0.22	0.14	0.12
		Right	0.53	0.54	0.56	0.55	0.42	0.44
	250	Left	0.21	0.18	0.22	0.2	0.14	0.09
		Right	0.54	0.52	0.55	0.54	0.52	0.41
R350 HT	175	Left	0.15	0.13	0.18	0.16	0.05	0.03
		Right	0.45	0.45	0.48	0.47	0.31	0.32
	250	Left	0.15	0.11	0.17	0.13	0.06	0
		Right	0.45	0.43	0.46	0.44	0.29	0.29

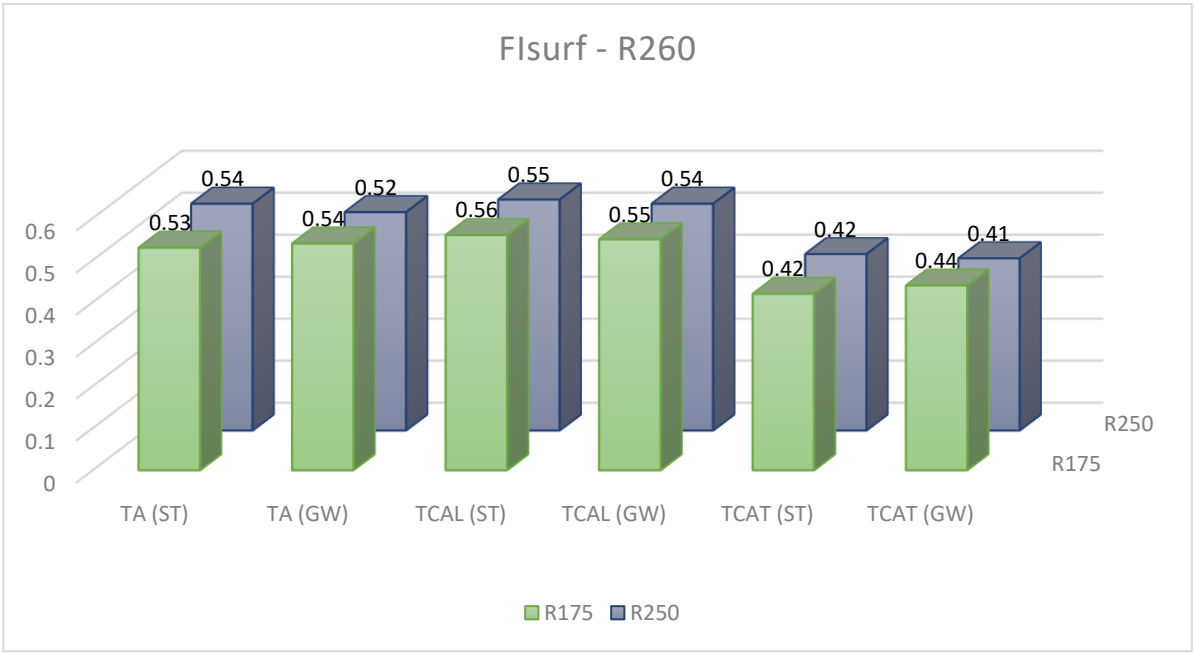

Figure 25 FIsurf of Train at Outer Wheel and Leading Axle with Material R260

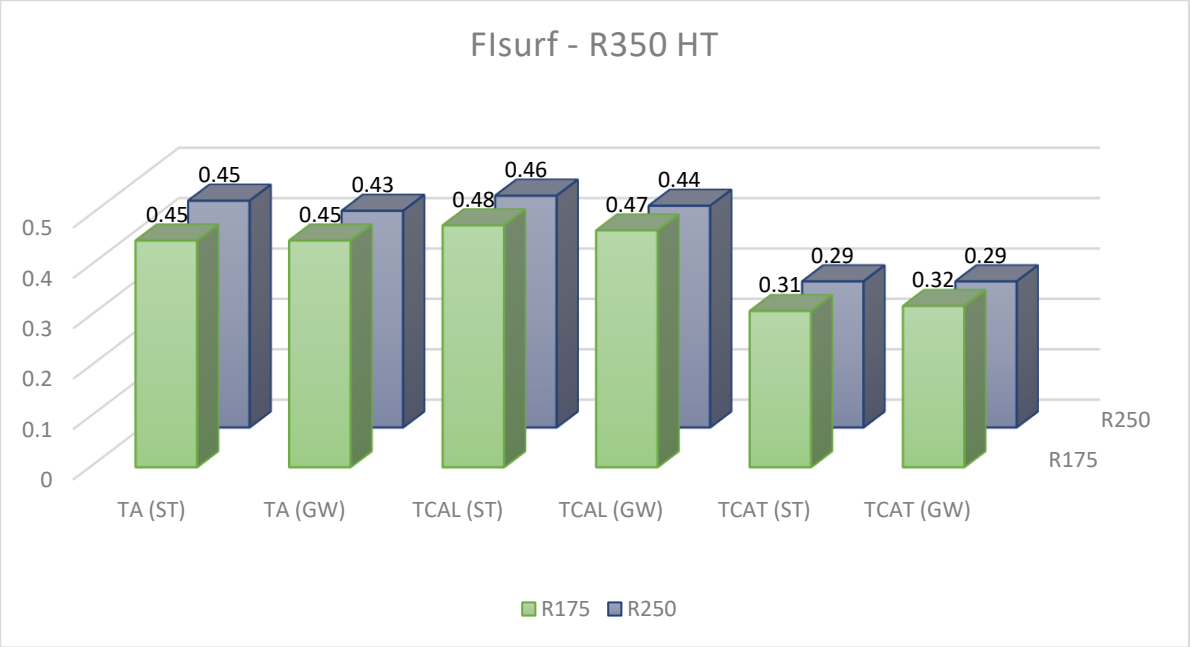

Figure 26 FIsurf of Train at Outer Wheel and Leading Axle with Material R350 HT

CHAPTER 5 CONCLUSION

The objective of the work was to analyze the effect of gauge widening on wear and rolling contact fatigue phenomena. To this aim a mathematical model of train track interaction was employed. Two different trains were analyzed, one for passenger transport and the other for freight transport. The effect of gauge widening on wear was investigated analyzing a global wear number, while for RCF two different models have been employed, one by Burstow [3] and the second by Ekberg.

Two parameters that commonly used for safety condition of derailment are Y/Q and ∑Y. All the trains are in safe region because Y/Q is lower than 1.2 (limit condition) and ∑Y is lower than limit condition for each train.

Simulation results show that gauge widening as a minor effect both on wear and RCF, as far as RCF is concerned the indications provided by the two models are often not coherent one with the other. The model by Ekberg is more detailed with respect to Burstow model, but on the other hand, it does not take into account the material removal due to wear which may inhibit crack propagation.

REFERENCES

[1] A. Ekberg, E. Kabo, Fatigue of railway wheels and rails under rolling contact and thermal loading-an overview, Wear 258 (2005) 1288-1300.

[2] A. Ekberg, E. Kabo, H. Andersson, An engineering model for prediction of rolling contact fatigue of railway wheels, Fatigue Frac. Eng. Mater. Struct. 25 (2002) 899-909.

[3] M.C. Burstow, Whole Life Rail Model Application and Development for RSSB-Continued Development of an RCF Damage Parameter, Rail Standards and Safety Board, London, 2004.

[4] Roger Enblom (2009) Deterioration mechanisms in the wheel–rail interface with focus on wear prediction: a literature review, Vehicle System Dynamics, 47:6, 661-700, DOI: 10.1080/00423110802331559

[5] M.C. Burstow, Whole Life Rail Model Application and Development for RSSB-Development of an RCF Damage Parameter, Rail Standards and Safety Board, London, 2003

[6] H. Hertz, Über die Berührung zweier fester, elastischer Körper, J. reine angew. Math. 92 (1882), pp. 156–171

[7] J.J. Kalker, On the rolling contact of two elastic bodies in the presence of dry friction, Doctoral thesis, Delft University of Technology, Delft, 1967

[8] Kalker, J. J., A strip theory for rolling with slip and spin, Proc. Kon. Nederlandse Akademie van Wetenachappen, Amsterdam, B70, pp. 10– 62, 1966

[9] Vermeulen, P. J. and Johnson, K. L., Contact of nonspherical elastic bodies transmitting tangential forces, Trans. ASME, 1964, June

[10] Iwnicki, S. (2006). Handbook of Railway Vehicle Dynamics. Taylor & Francis Group.

[11] J.J. Kalker, Rolling contact phenomena – linear elasticity, in CISM International Centre for Mechanical Sciences, Vol. 411, Springer, New York, 2001, ISBN: 3-211-83332-3.

[12] Francesco Braghin , Stefano Bruni & Giorgio Diana (2006) Experimental and numerical investigation on the derailment of a railway wheelset with solid axle, Vehicle System Dynamics, 44:4, 305-325

[13] Shust, W.C., Elkins, J.A., Kalay, S., and El-Sibaie, M., Wheel-Climb Derailment Tests using AAR's Track Loading Vehicle, Association of American Railroads Report R-910, December 1997

[14] UIC Code 518: Testing and Approval of Railway Vehicles from the Point of View of their Dynamic Behaviour– Safety–Track Fatigue–Ride Quality, International Union of Railways, 3rd ed., Paris, October 2005.

[15] EN 14363: Railway Applications — Testing for the Acceptance of Running Characteristics of Railway Vehicles — Testing of Running Behaviour and Stationary Tests, CEN, Brussels, June 2005

[16] A.F. Bower, K.L. Johnson, Plastic flow and shakedown of the rail surface in repeated wheel–rail contact, Wear 144 (1991) 1–18

[17] K.L. Johnson, The strength of surfaces in rolling contact, Proc. Inst. Mech. Eng. 203 (1989) 151–163

[18] J. Tunna, J. Sinclair, J. Perez, A review of wheel wear and rolling contact fatigue, Proc. IMechE F: J. Rail Rapid Trans. 221 (2007) 271–289.